IEEE Journal of Microwaves

Received 25 January 2023; revised 9 March 2023; accepted 14 March 2023.

Digital Object Identifier 10.1109/JMW.2023.3261901

Near-Field Microwave Microscopy for 3D Surface Assessment of Manufactured Structures

D. R. JONES [1], P. BROWN [2], G. MCFARLAND[2], R. PERKS[1], H. CHOI[1], S. CRIPPS [1] (Life Fellow, IEEE), AND A. PORCH [1]

(Regular Paper)

[1]School of Engineering, Cardiff University, CF24 3AA Cardiff, U.K.
[2]Renishaw plc., GL12 8JR New Mills, U.K.

CORRESPONDING AUTHOR: D. R. Jones (e-mail: jonesdr11@cardiff.ac.uk).

ABSTRACT Using near-field scanning microwave microscopy as a contact and non-contacting investigative tool for 3D surface metrology with three differing measurement modes, it has been possible to analyse structures that may be difficult for existing metrology systems. The system utilizes the small change in capacitance between a coaxial resonant probe (at around 2 GHz) ending in an open circuit tip, and the sample surface. This is measured in the frequency domain by the shift in the resonance frequency of the voltage transmission coefficient $|S_{21}|$. It is also possible to investigate various materials (metallics, plastics etc.) owing to their differing dielectric properties. The probe has been tested on a computer-controlled 3D stage but is suitable for incorporation into a commercial co-ordinate measurement machine (CMM) to enhance its capability to inspect the inside surfaces of structures, e.g., threads in small bores.

INDEX TERMS 3D metrology scan, near-field microwave microscopy, thread analysis.

I. INTRODUCTION

Generating a 3D image of a component's surface can give a comprehensive analysis of the structure, which can be helpful in determining manufacturing errors and common failures. 3D measurements of some small structures can be difficult due to their size and shape, examples being screw threads and bores, which are used extensively to connect components and are one of the most commonly used fasteners due to high strength and the ease of disconnecting [1]. Assessing these threads can be difficult due to the nature of the geometry of the thread; for example, when using touch probes with a spherical tip, it can be difficult to accurately represent the thread profile, especially in the root [2]. Other methods, such as profilometers, become less accurate with wear [3] and are inflexible in their measurement capabilities. Although threads come in a variety of tolerances, accurate threads become more important for the performance of some applications [4]. The main commercially available tools are manual go/no-go gauges [5] , micrometre measuring systems [6] or manual extendable touch probes [7]. These systems are largely manually operated and are therefore time consuming, also introducing an element of human error and being prone to variations between different operators. They are also manufactured to a specific thread size and tolerance, thus requiring several gauges that will wear with use. There are commercial systems and various studies which have been successful in investigating internal threads and bores, using optical measurement systems [4], eddy-currents [8] and laser measuring systems [9]. Whilst good for assessing fairly large bores (of diameter > 8 mm), these systems are yet to be proven with smaller bores.

Use of near-field microwave microscopy (NFMM) may be able to overcome some of the limitations of the other systems and can be used as a surface scanning tool, particularly to investigate small bores. An open circuit, resonant microwave probe is used for the scanning system reported here, which has a coupling layout similar to that used previously in resonant microfluidic devices [10]. Utilising a two-port coupling system and so measuring the voltage transmission coefficient between ports increases the dynamic range compared with a

one-port reflection measurement; this increases the precision of measurement of small shifts in resonant frequency caused by changes in capacitance of the probe's tip to sample system.

In this article the samples have homogeneous, bulk surface properties and so it is assumed that any change in resonant frequency comes from the change in tip-sample distance, not in the change of the dielectric properties of the material. Microwave losses (in terms of changes in the reciprocal of the quality factor Q) are not considered as the focus is solely on the surface topography, not on the characterisation of the material.

NFMM was first conceptualized by Synge in 1928 to overcome Abe's diffraction limit. Further research was then carried out by Ash and Nicholls in 1972, where an evanescent wave probe was used to study an object [11]. Since then there has been extensive NFMM research [12], [13], [14], [15], [16], [17], [18], resulting in nanoscale resolution [19], [20]. NFMM can be used for various disciplines in many applications, including analysing permittivity of nano structures [21], imaging of biological cells [22] and detecting defects buried in metallic samples [23]. The majority of NFMM probes reported in the literature end with a tip [24], [25], [26] or with an aperture [11], [27], together with others described in detail by Anlage et al. [28].

It is proposed that by using this technology, with various measuring modes described below, it is possible to analyse structures such as small thread bores. The probes can be miniaturised in a similar manner to [29], where a coaxial probe was fabricated with a diameter of less than 1mm. This system also has the capability to investigate various materials, with metals and high permittivity materials having the greatest frequency shift of the probe (and hence greatest contrast relative to air) owing to the greater electrical polarisation of the sample's surface induced by the microwave electric field emanating from the probe's tip. While plastics and other lower permittivity materials will result in a smaller frequency shift at a fixed tip-sample distance, there is still sufficient resolution in the measurements of resonant frequency to analyse structures fabricated from these materials.

II. PRINCIPLES

The resonant sensor used here is based on a half wavelength resonant section of coaxial cable which is open circuit at both ends. One end is terminated in a sharp tip that interacts capacitively with a sample in its vicinity. The other end is capacitively coupled to the input and output measurement ports by the T-section shown in Fig. 1, which enables measurement of the voltage transmission coefficient S_{21} in the frequency domain using a vector network analyser.

The probe resonates at harmonics of the fundamental resonant frequency governed by (1).

$$f = \frac{c}{2l\sqrt{\varepsilon_r}} \tag{1}$$

where f is the fundamental frequency, ε_r is the relative permittivity of the dielectric spacer (usually PTFE, around 2.1),

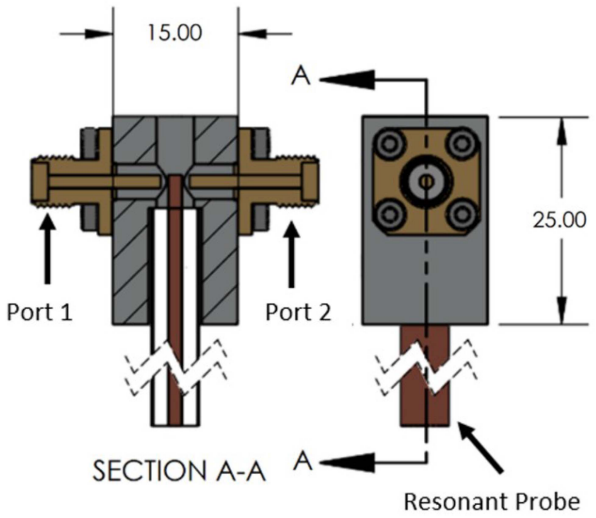

FIGURE 1. T-Connector for capacitively coupling into an open-ended resonant coaxial cable, consisting of two SMA connectors, coaxial cable, and an aluminium housing. Units in mm.

c is the speed of light in vacuo and l is the length of the centre conductor of the resonant probe.

As the probe tip comes into the vicinity of a sample, a small capacitance between the tip and surface is formed. There is no simple analytic formulation of this structure, but the simplest model is that of a parallel plate capacitor in the limit where the tip-sample separation d is comparable (or less than) the tip radius, so that the additional tip-sample capacitance is approximately that given by the simple formula (2), not accounting for the stray capacitance.

$$C_z \approx \frac{\varepsilon_0 A_{eff}}{d} \tag{2}$$

This assumes air-spacing, with A_{eff} being the effective area of the tip-sample capacitor. To first order, the rate of change of resonant frequency with d is then proportional to $1/\sqrt{d}$ (neglecting any change in effective area), as demonstrated in the experimental data of Fig. 2, collected using commercial rigid coaxial cables of various diameters. RG401 cable has an inner conductor diameter (ICD) of 1.63 mm and an outer conductor diameter (OCD) of 6.35 mm, RG402 ICD of 0.92 mm and OCD of 3.58 mm, whilst RG405 has ICD of 0.51 mm and OCD of 1.61 mm. This experiment used the inner conductor supplied, which is silver plated copper, and the spacer is PFTE in all cases.

The resolution of the measurement is enhanced by reducing the protruding tip radius, but any reduction in the radius of the centre conductor also reduces the quality factor (Q) of the resonance proportionately. To achieve a sharp, well-defined resonance, which is easy to excite, and which provides a noise-free measurement of $|S_{21}|$, a Q of above 100 is maintained for all probe sizes. The shift in resonant frequency from plots such as Fig. 2 is used to generate a topographical representation of surfaces. The measurement contrast improves the greater the difference in the relative permittivity of the

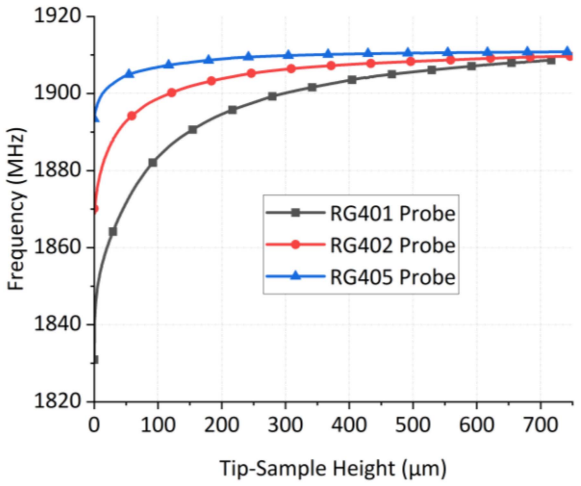

FIGURE 2. Frequency-height plot of a metallic sample and probes of RG405, RG402 and RG401 coaxial cables, demonstrating the higher contrast of frequency measurement for a larger diameter probe.

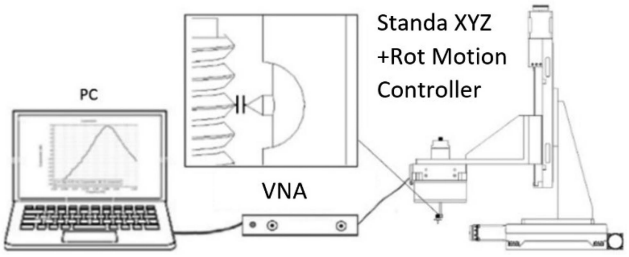

FIGURE 3. System setup consisting of XYZ+Rotary stage, connected to both VNA and PC using an RG405 side probe investigating an internal M6 thread.

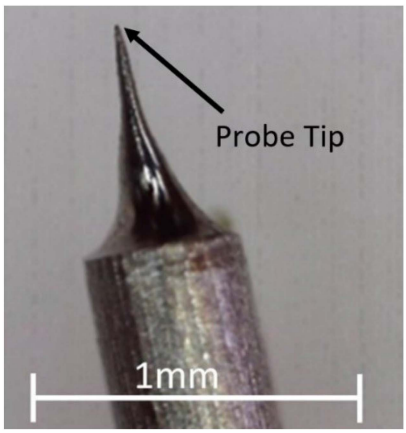

FIGURE 4. Result of the electrochemical etching of the tungsten inner conductor for a RG405 cable, which has a diameter of 0.5 mm.

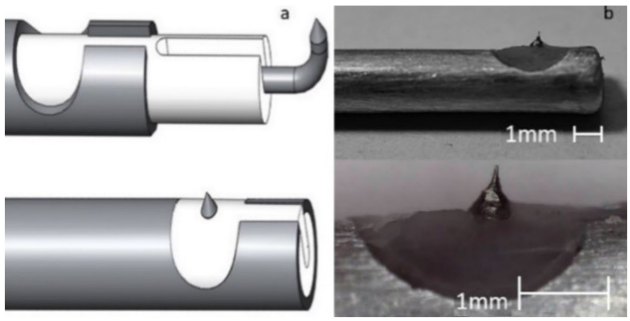

FIGURE 5. (a) 3D model of the construction of the side probe with the inner conductor replaced with a sharp right-angled tip, before being filled with paraffin wax; (b) photograph of a side probe made using RG405 coaxial cable.

FIGURE 6. Constant frequency scan of the tails side of a U.K. two-shilling coin.

sample compared with air. Hence, metals give the strongest response, but it is also possible to measure common plastics such as Nylon with reasonably high permittivity. In simple terms, it is possible to define a "contrast" factor of based on the polarisation of the surface as $(\varepsilon - 1)/(\varepsilon + 1)$, which equals 1 for metals, around 0.64 for Nylon ($\varepsilon = 4.5$) and 0.35 for PTFE ($\varepsilon = 2.1$).

III. SYSTEM SET-UP

As shown in Fig. 3 , the T-coupling structure (of Fig. 1) and its resonant probe is mounted into an aluminium housing that fits onto a Standa XYZ and rotary motion controller. The motion controller has a linear minimum increment of 0.31 μm and minimum rotational increment of 360 arcsec. The probe is connected to a vector network analyser (Copper Mountain M5065), which measures the voltage transmission coefficient S_{21}. Both VNA and stage are controlled by a laptop computer running National Instruments LabVIEW software, which synchronises probe position and microwave measurements.

IV. PROBE MANUFACTURING

While the previous experiments used probes with sharpened, silver-plated, copper inner conductors, for the remaining smaller probe experiments the probe is manufactured from a length of commercial coaxial cable whose centre conductor has been removed and replaced with a tungsten wire, which is amenable for etching into a sharp tip. An electrochemical etching method was used, as described by Prasad and Singh [30]. The tungsten wire is etched at the meniscus, creating a sharp tip once drop-off has occurred. The entire silver-plated copper inner conductor of an RG405 cable is removed and

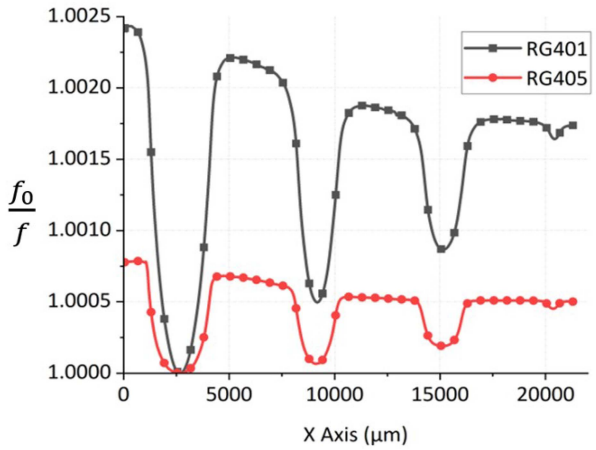

FIGURE 7. Plot of measured frequency using RG401 and RG405 analysing a rubert 513 sample.

FIGURE 8. A Rubert 513 calibrated specimen formed of Nickel, used as a comparison gauge between measurement modes.

replaced with this sharply tipped tungsten wire, shown in Fig. 4 with a tip diameter of approx. 15 μm, thus forming the basis of the resonant, open-ended probe.

Manufacturing a sharp tip is important as it focuses the electric field onto the location of interest. The larger the tip radius, the more the electric field becomes dispersed and this, therefore, reduces the resolution of the scanning system, although also increasing the contrast. It is therefore important to choose the right tip for increased contrast or resolution for the specific measurement required.

A novel side-angled probe has also been developed, with the capability of scanning relatively large undulating surfaces in small bores, such as found in internal threads; these surfaces are difficult to assess using conventional scanning methods. The side-angled probe is manufactured by removing the central conductor of a section of commercial coaxial cable, creating a small slit in the bottom of the outer conductor, and removing the outer conductor where side probe protrudes to minimise coupling between the inner and outer conductors. A tungsten wire is used as the inner conductor, as for the straight probe, and is electro-chemically etched at its end to form a sharp tip in the usual way. The tungsten wire is then bent at a

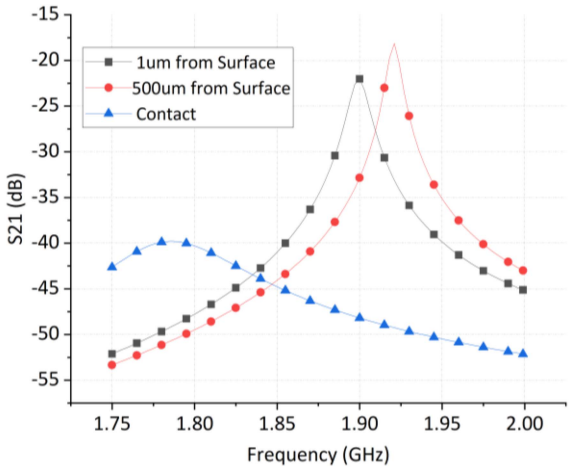

FIGURE 9. S_{21} measurements with 201 points per sweep, of a probe based on RG405 cable, showing the probe 500 μm, 1 μm and touching a metallic sample; the frequency and S21 decrease rapidly when contacting the metallic surface.

right angle to the axis of the probe and is re-inserted, with the removed PTFE refilled with paraffin wax, as shown in Fig. 5.

V. MEASUREMENT MODES

Three measurement modes are used to measure the surface topography.

1) CONSTANT FREQUENCY, VARY HEIGHT

A constant tip-sample distance can be maintained by measuring the probe's resonant frequency at a certain distance from the surface. The desired frequency is kept constant with constant feedback from the VNA and the motion controllers, which will adjust its z-axis position to maintain this frequency if the topography of the surface has changed since the previous measurement. This similar method has been used to image surfaces such as a coin in [24] although a VNA is used to track the resonant frequency from the S_{21} trace in this method to produce an image of a U.K. two-shilling coin in Fig. 6.

2) CONSTANT HEIGHT, VARY FREQUENCY

The motion controller will allow the probe to scan the surface at the desired step size and measure frequency continuously at a fixed value of z-coordinate (i.e., "fixed height"). As the surface topology varies, so will the probe's resonant frequency, increasing for larger probe-sample height. The frequency contrast is greater for the larger RG401 probe, as is shown in Fig. 7 of a scan of a Rubert 513 sample shown in Fig. 8, decreasing for the smaller RG405 probe. Using a tip-sample calibration plot, obtained first using a perfectly flat metal surface, it is possible to interpolate the frequency data into tip-distance data for a general sample.

3) TOUCH PROBE

Each probe is open ended and a capacitor is formed between the tip and sample that modifies the open circuit condition at

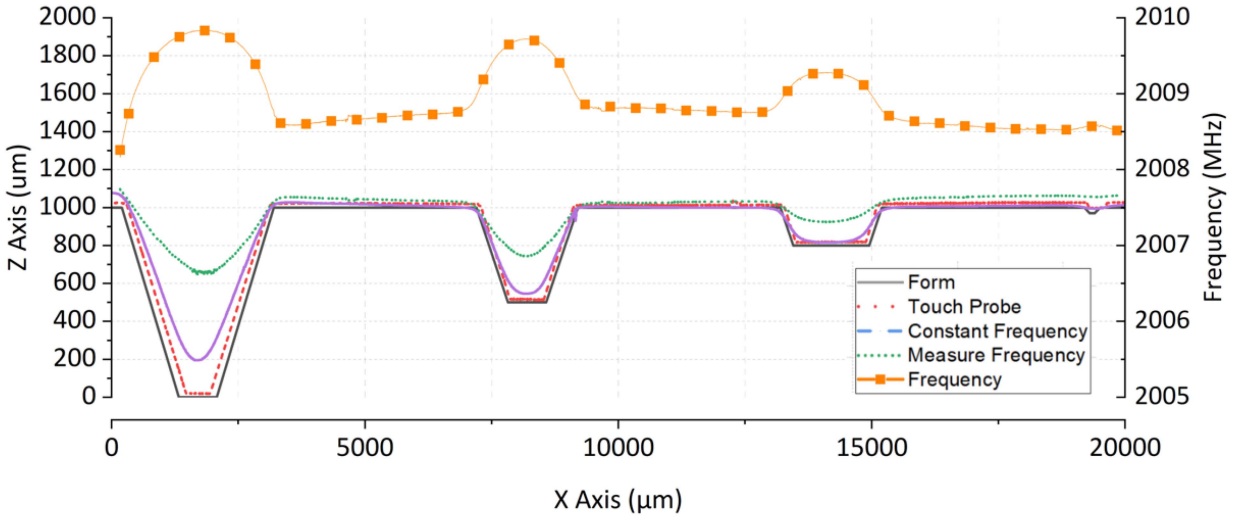

FIGURE 10. Comparison of the three modes of measurement with the same Nickel rubert 513 sample using an RG405 probe.

the sample end via a tip-sample capacitance. When the tip touches the metallic surface then this end of probe is effectively short circuited and the resonant frequency decreases dramatically (indeed, theoretically it should halve). The S_{21} COMSOL simulation of the probe at tip-sample distances of 500 μm, 1 μm and touching are shown in Fig. 9. Utilising this large reduction in frequency, it is possible to determine the surface topography by recording the motion controller's location on contact, though clearly care must be taken not to blunt the sharpened tip.

To compare the various modes of measurement, a precision reference nickel specimen was used (Fig. 8) and the scans were conducted using each mode; the results are shown in Fig. 10.

The mode which reproduces the surface topography the best is the touch mode (iii). The constant frequency mode (i) is less effective and becomes increasingly so the deeper the troughs in the surface topology become, although this has the advantage of being a non-contact measuring mode. Using the constant height mode (ii) is the quickest as it is an open loop system without feedback, so it is not constantly adjusting to the sample's undulating surface. Using a calibration plot such as that of Fig. 2 for the measuring frequency mode, the three mode frequency data can then be interpolated to gain an estimated height of the tip above the surface.

VI. SIDE-ANGLED PROBE

A COMSOL simulation is used to compare the straight and the side probes set-ups. Using a straight RG405 probe with an inner conductor of 50mm length with an extruding pointed tip of length 0.05mm gave the expected fundamental resonant frequency of 2.097 GHz. As shown in Fig. 11, the frequency reduced by 2.53 MHz when a copper sample was introduced 50 μm away from the tip compared with the tip in air.

A COMSOL simulation of the side probe is shown in Fig. 12; an inner conductor length of 45 mm gives the same

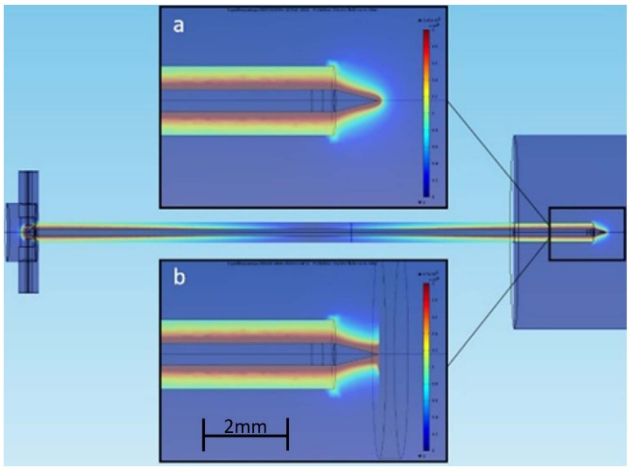

FIGURE 11. COMSOL simulation of a pointed RG405 coaxial cable, showing a frequency drop of 2.53 MHz between the probe in air (a), and when a cooper sample is introduced at a distance of 50 μm, (b).

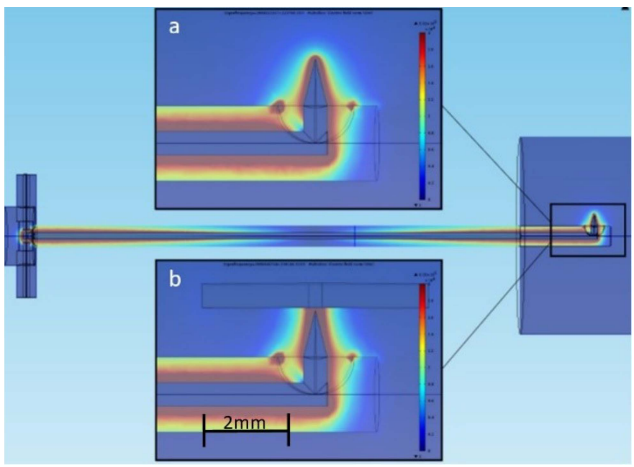

FIGURE 12. COMSOL simulation of RG405 side probe without sample (a) and with a sample 50 μm from tip (b).

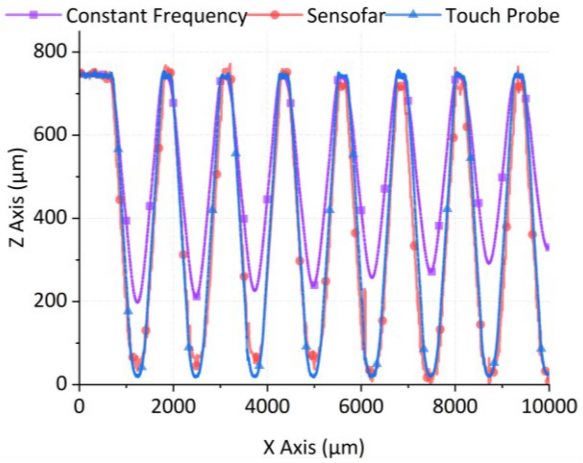

FIGURE 13. **M8 external thread measurement using constant frequency and touch probe modes compared with Sensofar measurements.**

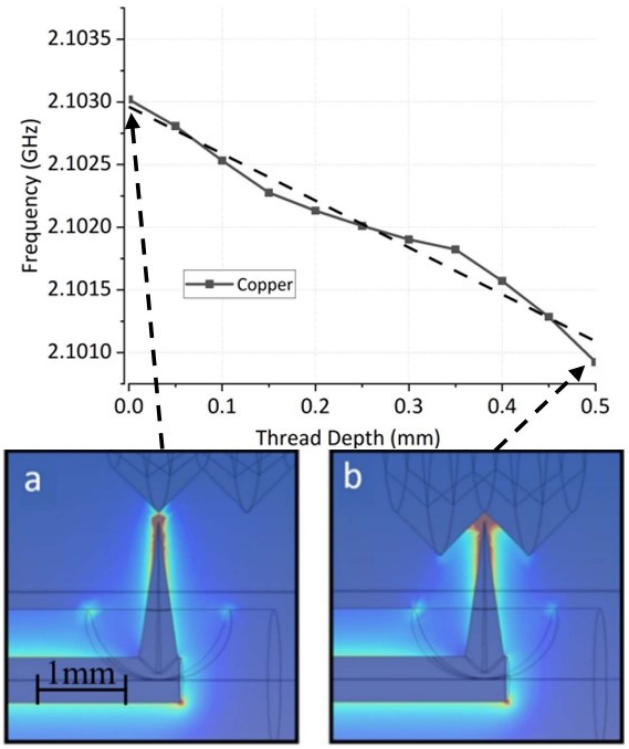

FIGURE 14. **COMSOL simulation at a constant 50 μm from surface for M8 thread, showing the varying frequency.**

resonant frequency as the straight probe of 2.097 GHz, the frequency decreasing by 1.72 MHz when a copper sample is introduced within 50 μm of the probe tip. This is compared with a 2.53 MHz decrease for the straight probe. Hence the side probe is less sensitive than the straight probe, due to the additional capacitive coupling between the inner and outer conductors near the tip.

The side probe was manufactured mainly to measure threads. To evaluate the capabilities of this system, an M8 thread was scanned using the contact and constant frequency scanning modes and compared with the scans from a Sensofar S mart scanning machine, which uses a conical measurement system. Using the Sensofar system required scanning analyses of the thread at various specified distances from the sample, which are then stitched together. This process was repeated six times, as its field of view is limited to 1.64 mm, and these results were then stitched together to produce a profile of the thread. This was compared with an image and the measurements taken from the microwave side-probe system, as shown in Fig. 13.

The overlaid data of two measurement systems demonstrates that the accuracy of the touch probe method is comparable with the Sensofar, although with the advantage of being a much more flexible measuring system. The non-contact, constant frequency measuring mode is also accurate at measuring the pitch of the thread, although the accuracy of the depth of the thread is limited, which was investigated further via COMSOL simulations.

As demonstrated in the COMSOL simulation of Fig. 14, at a constant tip-sample distance (50 μm) the frequency does not remain constant during the scan. This is due to the larger effective surface area at the trough of the thread compared to the crest, which increases the tip-sample capacitance and thus reduces the resonant frequency. This is not much of an issue with relatively flat surfaces, such as the coin scan shown in Fig. 6. Due to the change in frequency on scanning the thread it is not possible to maintain a constant tip-sample distance by maintaining a set frequency. As the frequency measured using the same tip-sample distance differs at the crest and the trough of the thread, due to a higher capacitance in the trough, it is difficult to accurately assess the thread using both constant frequency and constant height modes. For example, if the frequency was set at a height of 50 μm from the crest, then the tip doesn't get close enough to the trough to achieve an accurate measurement; conversely, if the frequency was set at 50 μm from the trough, this would mean the frequency would be much lower due to the higher capacitance achieved in the trough.

When the probe exits the higher electric field of the trough, it is not possible to achieve the original set frequency and when attempting to do so the probe will collide with the sample thread. To minimise this effect, it is possible to electrically shield most of the tip [31], leaving the apex of the tip to interact with the surface. However, this would have the downside of increasing the effective width of the inner conductor.

To demonstrate the 3D capability of the system an internal M6 thread was investigated using the touch probe method, due the reasons mentioned previously, using a commercially available RG405 coaxial cable manufactured to a side probe. The system scans down in the Z axis with step size of 2.5 μm before rotating 2 degrees and scans up the Z axis until the entire thread is scanned. This technique produced a 3D image of the internal M6 thread shown in Fig. 15.

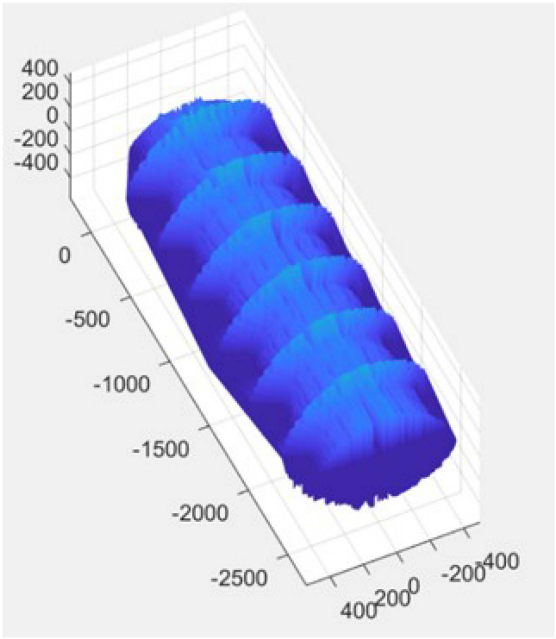

FIGURE 15. Internal M6 thread with 1 mm pitch, measured using the touch probe method and a commercially available RG405 coaxal manufactured into a side probe.

VII. CONCLUSION

Both straight and side-angled resonant microwave probes have been demonstrated for surface imaging; this could be further developed to analyse the enclosed surfaces of additive manufactured components, which would be hard to assess using other methods. The resulting measurement system has three measurement modes that can be used for different applications. The constant height method (where frequency is measured) is quick and could be used to determine an estimated profile of a surface and possibly for fault finding, such as identifying partial threads or swarf blockages, although without achieving a great understanding about the nature and geometry of the fault. Using the constant frequency method is useful if non-contact measurements are needed and has been shown to be effective up to a limiting feature depth; however, it is slower than the constant height method due to the continuous feedback required to maintain a constant tip-sample distance. Using the touch probe enables a higher accuracy profile to be produced and enables threads to be accurately analysed to measure flank angle, thread depth and pitch, which is a major advantage for small internal threads. Further development is required to make the microwave system more manufacturable and to achieve faster scanning times. Once small side-probes have been manufactured, further research will be carried out to investigate the internal surface topology of small bores (of < 3 mm in diameter).

REFERENCES

[1] G. Fromentin, G. Poulachon, A. Moisan, B. Julien, and J. Giessler, "Precision and surface integrity of threads obtained by form tapping," *Corporate Insolvency Resolution Process Ann.*, vol. 54, pp. 519–522, Dec. 2005, doi: 10.1016/S0007-8506(07)60159-0.

[2] C. C. Souza, L. J. Arantes, A. Piratelli-Filho, and R. V. Arencibia, "Assessment of the effect of stylus tip radius on milled, bored, and honed surfaces," *Int. J. Adv. Manuf. Technol.*, vol. 104, no. 5–8, pp. 2459–2471, Oct. 2019, doi: 10.1007/s00170-019-04083-5.

[3] V. Radhakrishnan, "Effect of stylus radius on the roughness values measured with tracing stylus instruments," *Wear*, vol. 16, no. 5, pp. 325–335, Nov. 1970, doi: 10.1016/0043-1648(70)90099-2.

[4] E. Hong, H. Zhang, R. Katz, and J. S. Agapiou, "Non-contact inspection of internal threads of machined parts," *Int. J. Adv. Manuf. Technol.*, vol. 62, no. 1–4, pp. 221–229, Sep. 2012, doi: 10.1007/s00170-011-3793-5.

[5] T. C. Folsom and P. D. Bondurant, "Non-contact internal thread inspection," SAE Int., Warrendale, PA, USA, SAE Tech. Paper 1999-01–3434, Oct. 1999, doi: 10.4271/1999-01-3434.

[6] E. S. Gadelmawla, "Development of computer vision algorithms for measurement and inspection of external screw threads," *J. Eng. Sci.*, vol. 39, no. 3, pp. 581–605, May 2011, doi: 10.21608/jesaun.2011.127666.

[7] Q. Tong, B. Han, D. Wang, J. Wang, Z. Ding, and F. Yuan, "A novel laser-based system for measuring internal thread parameters," *J. Russian Laser Res.*, vol. 35, no. 3, pp. 307–316, May 2014, doi: 10.1007/s10946-014-9429-0.

[8] P.-Y. Joubert, E. Vourc'h, and V. Thomas, "Experimental validation of an eddy current probe dedicated to the multi-frequency imaging of bore holes," *Sensors Actuators A, Phys.*, vol. 185, pp. 132–138, Oct. 2012, doi: 10.1016/j.sna.2012.07.009.

[9] H. Zhang, R. Katz, and J. Agapiou, "In-process inspection of internal threads of machined automotive parts," *Proc. SPIE*, vol. 7432, pp. 129–137, Aug. 2009, doi: 10.1117/12.824387.

[10] D. J. Rowe, A. Porch, D. A. Barrow, and C. J. Allender, "Microfluidic device for compositional analysis of solvent systems at microwave frequencies," *Sensors Actuators B, Chem.*, vol. 169, pp. 213–221, Jul. 2012, doi: 10.1016/j.snb.2012.04.069.

[11] E. A. Ash and G. Nicholls, "Super-resolution aperture scanning microscope," *Nature*, vol. 237, no. 5357, Jun. 1972, Art. no. 5357, doi: 10.1038/237510a0.

[12] F. Duewer, C. Gao, I. Takeuchi, and X.-D. Xiang, "Tip–sample distance feedback control in a scanning evanescent microwave microscope," *Appl. Phys. Lett.*, vol. 74, no. 18, pp. 2696–2698, May 1999, doi: 10.1063/1.123940.

[13] S. Hong, J. Kim, W. Park, and K. Lee, "Improved surface imaging with a near-field scanning microwave microscope using a tunable resonator," *Appl. Phys. Lett.*, vol. 80, no. 3, pp. 524–526, Jan. 2002, doi: 10.1063/1.1435068.

[14] S. Geaney et al., "Near-field scanning microwave microscopy in the single photon regime," *Sci. Rep.*, vol. 9, no. 1, pp. 1–7, Aug. 2019, doi: 10.1038/s41598-019-48780-3.

[15] J. Lee, C. J. Long, H. Yang, X.-D. Xiang, and I. Takeuchi, "Atomic resolution imaging at 2.5 GHz using near-field microwave microscopy," *Appl. Phys. Lett.*, vol. 97, no. 18, Nov. 2010, Art. no. 183111, doi: 10.1063/1.3514243.

[16] N. Okazaki et al., "Development of scanning microwave microscope with a lumped-constant resonator probe for high-throughput characterization of combinatorial dielectric materials," *Appl. Surf. Sci.*, vol. 189, no. 3/4, pp. 222–226, Apr. 2002, doi: 10.1016/S0169-4332(01)01013-3.

[17] A. Tselev, S. M. Anlage, H. M. Christen, R. L. Moreland, V. V. Talanov, and A. R. Schwartz, "Near-field microwave microscope with improved sensitivity and spatial resolution," *Rev. Sci. Instrum.*, vol. 74, no. 6, pp. 3167–3170, Jun. 2003, doi: 10.1063/1.1571954.

[18] R. Kantor and I. V. Shvets, "Method of increasing spatial resolution of the scanning near-field microwave microscopy," *J. Appl. Phys.*, vol. 93, no. 9, pp. 4979–4985, May 2003, doi: 10.1063/1.1522486.

[19] A. Imtiaz, S. M. Anlage, J. D. Barry, and J. Melngailis, "Nanometer-scale material contrast imaging with a near-field microwave microscope," *Appl. Phys. Lett.*, vol. 90, no. 14, Apr. 2007, Art. no. 143106, doi: 10.1063/1.2719164.

[20] A. Kramer, F. Keilmann, B. Knoll, and R. Guckenberger, "The coaxial tip as a nano-antenna for scanning near-field microwave transmission microscopy," *Micron*, vol. 27, no. 6, pp. 413–417, Dec. 1996, doi: 10.1016/S0968-4328(96)00047-9.

[21] W. Guo, H. Xo, W. Liang, and Q. Gao, "Quantitative study of near-field microwave microscopy: Application to metrology of dielectrics at nanoscale," in *Proc. Cross Strait Radio Sci. Wireless Technol. Conf.*, 2021, pp. 55–57, doi: 10.1109/CSRSWTC52801.2021.9631712.

[22] M. Farina et al., "Inverted scanning microwave microscope for in vitro imaging and characterization of biological cells," *Appl. Phys. Lett.*, vol. 114, no. 9, Mar. 2019, Art. no. 093703, doi: 10.1063/1.5086259.

[23] C. Plassard et al., "Detection of defects buried in metallic samples by scanning microwave microscopy," *Phys. Rev. B*, vol. 83, no. 12, Mar. 2011, Art. no. 121409, doi: 10.1103/PhysRevB.83.121409.

[24] C. P. Vlahacos, D. E. Steinhauer, S. K. Dutta, B. J. Feenstra, S. M. Anlage, and F. C. Wellstood, "Quantitative topographic imaging using a near-field scanning microwave microscope," *Appl. Phys. Lett.*, vol. 72, no. 14, pp. 1778–1780, Apr. 1998, doi: 10.1063/1.121182.

[25] D. E. Steinhauer, C. P. Vlahacos, S. K. Dutta, F. C. Wellstood, and S. M. Anlage, "Surface resistance imaging with a scanning near-field microwave microscope," *Appl. Phys. Lett.*, vol. 71, no. 12, pp. 1736–1738, Sep. 1997, doi: 10.1063/1.120020.

[26] C. P. Vlahacos, R. C. Black, S. M. Anlage, A. Amar, and F. C. Wellstood, "Near-field scanning microwave microscope with 100 μm resolution," *Appl. Phys. Lett.*, vol. 69, no. 21, pp. 3272–3274, Nov. 1996, doi: 10.1063/1.118033.

[27] M. Abu-Teir, M. Golosovsky, D. Davidov, A. Frenkel, and H. Goldberger, "Near-field scanning microwave probe based on a dielectric resonator," *Rev. Sci. Instrum.*, vol. 72, no. 4, pp. 2073–2079, Apr. 2001, doi: 10.1063/1.1351837.

[28] S. M. Anlage, V. V. Talanov, and A. R. Schwartz, "Principles of near-field microwave microscopy," in *Scanning Probe Microscopy*, S. Kalinin and A. Gruverman, Eds., Berlin Germany: Springer, 2007, pp. 215–253, doi: 10.1007/978-0-387-28668-6_8.

[29] N. Dehghan, A. Porch, S. C. Cripps, and P. H. Aaen, "A novel high resolution E-field microscope system with applications in HPA diagnostics," in *Proc. 78th ARFTG Microw. Meas. Conf.*, 2011, pp. 1–3, doi: 10.1109/ARFTG78.2011.6183871.

[30] R. K. Prasad and D. K. Singh, "Low cost electrical probe station using etched tungsten nanoprobes: Role of cathode geometry," *Nano Exp.*, vol. 1, no. 2, Sep. 2020, Art. no. 020042, doi: 10.1088/2632-959X/abb6c4.

[31] Š. Lányi, J. Török, and P. Řehůřek, "A novel capacitance microscope," *Rev. Sci. Instrum.*, vol. 65, no. 7, pp. 2258–2261, Jul. 1994, doi: 10.1063/1.1144738.